JOURNAL OF SOLID STATE CHEMISTRY 74, 117–125 (1988)

# Improvement of $CaFe_2O_4$ Photocathode by Doping with Na and Mg

YASUMICHI MATSUMOTO, KAZUYOSHI SUGIYAMA, AND EI-ICHI SATO

*Department of Industrial Chemistry, Faculty of Engineering, Utsunomiya University, Ishi-icho 2753, Utsunomiya 321, Japan*

Received May 4, 1987; in revised form October 14, 1987

The low conductivity of $CaFe_2O_4$ and the nonohmic contact in the $CaFe_2O_4$/metal interface, which lead to only a small photocurrent, were improved by doping with Na and Mg. The oxides of the $Ca_{1-x}Na_x$ $Fe_{2-y}Mg_yO_4$ system gave the high conductivity and the ohmic contact of the oxide/Pt–Pd interface, but very small photocurrent. It was judged from the measurement of the Seebeck coefficient that the hopping mechanism is dominant for the conduction of the oxides containing Na. The hopping level is presumed to bring about the ohmic contact and the very small photocurrent because of the small band bending. The $CaFe_2O_4$/Na,Mg electrode, where one side of the surfaces was doped with Na and Mg and the interface of $CaFe_2O_4$/Na,Mg/Pt–Pd was ohmic contact, gave a large photocurrent. Photoelectrochemical dissolution was observed for the $CaFe_2O_4$/Na,Mg electrode in acidic solution but not in neutral solution. The mechanism of the dissolution is also discussed. 

## Introduction

The oxide semiconductors with Fe in the lattice have relatively narrow band gaps (2.1 ± 0.2 eV) (*1–15*) and therefore are promising as photoelectrode material in water photolysis. Turner *et al.* (*13*) reported the production of $H_2$ from water by illumination of both electrodes in a Mg-doped (*p*-type) and Si-doped (*n*-type) iron oxide assembly. The *p*-type $CaFe_2O_4$ semiconductor is a suitable photocathode material for photolysis of water by a *p*/*n* assembly, because of its stability in neutral solution and relatively narrow band gap (1.9 eV) (*15*). However, the quantum efficiency is still relatively small, although the increase of this efficiency was observed in acidic solution owing to a large band bending (*16*). There are two main reasons for the small photocurrent for this electrode in addition to the band bending. One is the nonohmic contact between the $CaFe_2O_4$ surface and the noble metals (Au, Pt–Pd alloy) which have large values in the work function (4.6 eV for Au and 5.4 eV for Pt–Pd) (*15, 16*): therefore, the interface of the $CaFe_2O_4$/Au or Pt–Pd alloy is a barrier for the large current. The other is poor conductivity of the $CaFe_2O_4$ bulk ($10^4$–$10^5$ Ω cm) (*15*).

The bulk conductivity of $CaFe_2O_4$ will be improved by the doping of other metal cations, $A^+$ and $B^{2+}$, if $A^+$ and $B^{2+}$ cations are substituted for Ca and Fe, respectively, as follows.

$$Ca^{2+}_{1-x}A^{+}_{x}Fe^{3+}_{2-x-2y}Fe^{4+}_{x+y}B^{2+}_{y}O_4 \qquad (1)$$

$$Fe^{4+} \rightarrow Fe^{3+} + h^+ \qquad (2)$$

The $Fe^{4+}$ produced by Eq. (1) will act as an acceptor to create a hole in the valence



0022-4596/88 $3.00

band as Eq. (2) shows. Consequently, the above substitution will bring about an increase in the conductivity of $CaFe_2O_4$.

In this paper, the $Na^+$ and $Mg^{2+}$ cations were used as the dopants $A^+$ and $B^{2+}$, respectively, because the ionic radii of $Na^+$ and $Mg^{2+}$ are almost the same as those of the $Ca^{2+}$ and $Fe^{3+}$ cations, respectively. The conductivities of $Ca_{1-x}Na_xFe_{2-y}Mg_yO_4$ were very high compared with those of $CaFe_2O_4$, and the ohmic contacts of the above doped oxides/noble metals were also observed, as described in the latter section. However, the photocurrent largely decreased by the above doping. Therefore, the sample, $CaFe_2O_4$/Na,Mg/metal, whose one side surface in contact with the noble metals was doped, was also used as the photocathode in the photoelectrochemical measurement. This electrode gave a large photocurrent as expected. The photoelectrochemical properties as well as the electrical properties of $CaFe_2O_4$ doped with Na and Mg are also demonstrated.

## Experimental

$CaFe_2O_4$ and $Ca_{1-x}Na_xFe_{2-y}O_4$ pellets were prepared as described in a previous paper (*15, 16*). Solutions of metal nitrates were used as the starting materials. The mixed solutions were evaporated to dryness and then heated at 900°C. The samples were sintered at 1200°C in air followed by oxidation in $O_2$ at 1000°C. The thicknesses were 0.6 mm for all sintering samples. In the preparation of $CaFe_2O_4$/Na,Mg, $Na^+$ and $Mg^{2+}$ were doped onto the surface of $CaFe_2O_4$ by thermal decomposition of Na and Mg mixed nitrates at 1000°C in $O_2$. In this case, the concentrations of the $Na^+$ and $Mg^{2+}$ cations were $10^{-5}$ and $10^{-4}$ mole/cm$^2$. Au or Pt–Pd (15%) alloy film was attached to one or both sides of the $CaFe_2O_4$ surfaces by the sputtering method (Ion Coater, Eiko Ltd.). A lead was then attached to the metal film with silver paste.

A 500-W Xenon lamp was used as the light source. The solutions used in the electrochemical measurements were 0.1 *M* $H_2SO_4$ and 0.25 *M* $K_2SO_4$ which were saturated with $N_2$. A SCE and a Pt plate were used as the reference and the counter electrodes, respectively. The electrode potentials quoted in this paper were recalculated to the reversible hydrogen electrode (RHE) scale, unless otherwise stated. Impedance measurements of the cell oxide electrode/electrolyte/Pt system were made with a frequency response analyzer (S-5720C, NF Electronic Instruments) operating in a frequency range from 100 kHz to 100Hz. Ca and Fe cations dissolved from the electrode into solutions were analyzed by inductively coupled plasma atomic emission spectroscopy (Seiko Instruments and Electronics). The XPS measurements were performed in an ESCA (Shimazu, Ltd.) using nonmonochromatized Mg$K\alpha$ radiation. The surface of the sample was sputtered by Ar ion in the measurement of the shallow part (<1 $\mu$m from the surface), while the surface was mechanically polished in the measurement of the deep part (>10 $\mu$m from the surface).

## Results and Discussion

### *Electrical and Photoelectrical Properties*

Table I shows the conductivities, $\sigma$, and the Seebeck coefficients, $Q$, of the $CaFe_2O_4$ samples doped with Na and/or Mg cations. The conductivity increases by the dopings of Na and Mg cations, but saturates at about 0.01–0.05 of $x$ in $Ca_{1-x}Na_xFe_2O_4$ and $CaFe_{2-x}Mg_xO_4$. The typical temperature dependence of the conductivity of $Ca_{0.9}Na_{0.1}Fe_{1.8}Mg_{0.2}O_4$ is shown in Fig. 1. The activation energy is 0.2 eV. The activation energies of other doped samples are in the range 0.13–0.24 eV and are smaller than that of the nondoped $CaFe_2O_4$ (0.4 eV) (*15*). The activation energies of the positive Seebeck coefficients were almost the same (0.15–

TABLE I

CONDUCTIVITIES AND SEEBECK COEFFICIENTS OF THE OXIDES AT 25°C

| Oxide | Conductivity ($\Omega^{-1} \cdot cm^{-1}$) | Seebeck coefficient ($mV \cdot K^{-1}$) |
|---|---|---|
| $CaFeO_4$ | $0.2–7.0 \times 10^{-5}$ | 2.5 |
| $Ca_{0.98}Na_{0.02}Fe_2O_4$ | $8.2 \times 10^{-3}$ | 0.90 |
| $Ca_{0.95}Na_{0.05}Fe_2O_4$ | $1.2 \times 10^{-2}$ | 0.71 |
| $Ca_{0.8}Na_{0.2}Fe_2O_4$ | $8.0 \times 10^{-3}$ | 0.73 |
| $Ca_{0.6}Na_{0.4}Fe_2O_4$ | $4.7 \times 10^{-3}$ | 1.00 |
| $CaFe_{1.99}Mg_{0.01}O_4$ | $1.2 \times 10^{-3}$ | 1.33 |
| $CaFe_{1.95}Mg_{0.05}O_4$ | $1.2 \times 10^{-3}$ | 1.70 |
| $CaFe_{1.9}Mg_{0.1}O_4$ | $6.6 \times 10^{-4}$ | 1.75 |
| $CaFe_{1.8}Mg_{0.2}O_4$ | $4.1 \times 10^{-4}$ | 1.60 |
| $Ca_{0.9}Na_{0.1}Fe_{1.8}Mg_{0.2}O_4$ | $3.0 \times 10^{-2}$ | 0.68 |
| $Ca_{0.98}Na_{0.02}Fe_{1.8}Mg_{0.2}O_4$ | $6.2 \times 10^{-3}$ | 0.70 |

0.24 eV) as those of the conductivities for the $CaFe_{2-x}Mg_xO_4$ samples, but about 0 eV for the samples containing Na. The typical temperature dependence of the Seebeck coefficient for $CaFe_{2.95}Mg_{0.05}O_4$ is shown in Fig. 2. The energy difference between the top of the valence level ($eg\downarrow$) and the

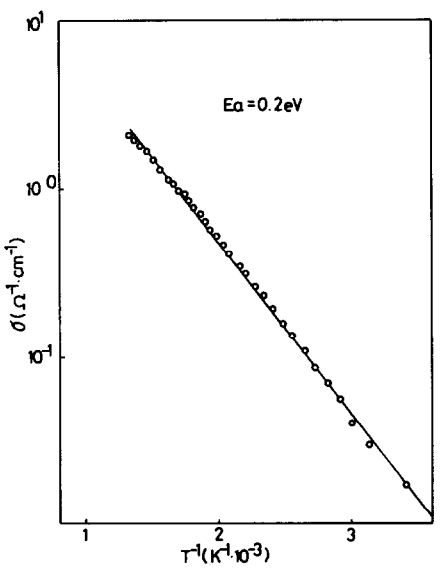


FIG. 1. Conductivity of $Ca_{0.9}Na_{0.1}Fe_{1.8}Mg_{0.2}O_4$ as a function of $T^{-1}$.

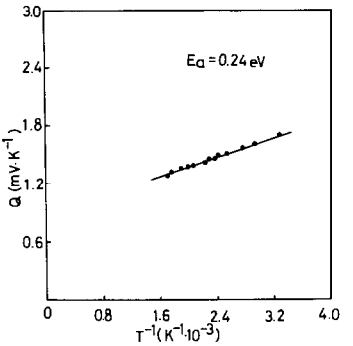


FIG. 2. Seebeck coefficient of $CaFe_{1.95}Mg_{0.05}O_4$ as a function of $T^{-1}$.

Fermi level is estimated to be 0.2 eV from the above activation energies for the $CaFe_{2-x}Mg_xO_4$ samples. On the other hand, it is suggested from the temperature independence of the Seebeck coefficient as stated above that, for the oxides containing Na, the hopping mechanism of the hole created by Eq. (2) is dominant for the conduction. The carrier concentration can be calculated by the following equation for the hopping conduction, if the contribution of the electron to the conduction is neglected,

$$Q = (k/e)\ln(N/p), \tag{3}$$

where $p$ is the carrier concentration, $N$ the density of states which is taken equal to the transition metal ion concentration ($6.7 \times 10^{21}$ $cm^{-3}$ for $CaFe_2O_4$ (*17*)) and $k$ the Boltzman constant. The mobility, $\mu$, of the hole can be calculated by using the following equation for the conductivity.

$$\sigma = ep\mu \tag{4}$$

Figure 3 shows $p$ and $\mu$ as a function of $x$ in $Ca_{1-x}Na_xFe_2O_4$ and $Ca_{1-x}Na_xFe_{1.8}Mg_{0.2}O_4$. The carrier concentration shows a maximum in the range $x = 0.05–0.2$. The decrease of the carrier in the range $0.2 < x$ will be based on the formation of the oxygen vacancy in the lattice which leads to the decrease of the $Fe^{4+}$ in Eq. (2). This is the main reason for the saturation of the

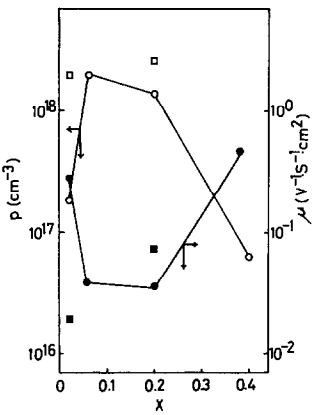


FIG. 3. Carrier concentrations (open symbols) and mobilities (closed symbols) of $Ca_{1-x}Na_xFe_2O_4$ (circles) and $Ca_{1-x}Na_xFe_{1.8}Mg_{0.2}O_4$ (squares) as a function of $x$.

conductivity with $x$ in $Ca_{1-x}Na_xFe_2O_4$. The same explanation can probably also be applied to the saturation of the conductivity with $x$ in $CaFe_{2-x}Mg_xO_4$ samples. The energy position of the hopping level in the oxides with Na will be situated in energy near the $eg\downarrow$ valence level in energy, since the position of the $Fe^{4+}$ corresponds to the $eg\downarrow$ valence band in energy (*16*).

Table II shows the photovoltages of the doped samples under the illumination of a 500-W Xenon lamp (340 mW/cm$^2$). In this measurement, the electrode system in Fig. 4 was used, and the photovoltage of the illuminated surface was referenced to the back surface. The thicknesses of the sputtered Pt–Pd films on the dark surface and the light surface were 250 and 150 Å, respectively. The transmittance of the 150-Å Pt–Pd film was about 20%. The photovoltage decreases with the dopings of Na and/or Mg, as Table II shows. In particular, it should be noted that the photovoltages of the oxides containing Na are very small compared with nondoped $CaFe_2O_4$. This suggests that the band bending in the space charge layer of these oxides is very small and that the interface between these oxides and the Pt–Pd alloy is close to an ohmic contact. This doping effect on the photovoltage is remarkable for the $CaFe_2O_4$ sample whose one side surface was doped with Na and Mg, i.e., the $CaFe_2O_4$/Na,Mg sample. The photovoltage measured at the nondoped surface is −200–300 mV, while that at the doped surface is 0–5 mV, as shown in Table II. The small band bending of the oxides containing Na in the lattice will be brought about by the formation of the hopping level which is near the $eg\downarrow$ valence level in energy as stated above. The Fermi level will be fixed at the hopping level, if the density of the hopping level is large, leading to the ohmic contact for samples such as $Ca_{0.95}Na_{0.05}Fe_2O_4$ and $Ca_{0.9}Na_{0.1}Fe_{1.8}Mg_{0.2}O_4$.

TABLE II

PHOTOVOLTAGES OF THE OXIDES UNDER THE ILLUMINATION OF A 500-W XENON (340 MW/CM$^2$)

| Oxide | Photovoltage (mV) |
|---|---|
| $CaFe_2O_4$ | −250–−300 |
| $Ca_{0.98}Na_{0.02}Fe_2O_4$ | −30–−40 |
| $Ca_{0.95}Na_{0.05}Fe_2O_4$ | −10–−20 |
| $Ca_{0.8}Na_{0.2}Fe_2O_4$ | −60–−100 |
| $CaFe_{1.99}Mg_{0.01}O_4$ | −250–300 |
| $CaFe_{1.95}Mg_{0.05}O_4$ | −150 |
| $CaFe_{1.9}Mg_{0.1}O_4$ | −160 |
| $CaFe_{1.8}Mg_{0.2}O_4$ | −60–−100 |
| $Ca_{0.9}Na_{0.1}Fe_{1.8}Mg_{0.2}O_4$ | −10–−20 |
| $Ca_{0.98}Na_{0.02}Fe_{1.8}Mg_{0.2}O_4$ | −50 |
| Doped surface of $CaFe_2O_4$/Na,Mg | 0–−5 |
| Nondoped surface of $CaFe_2O_4$/Na,Mg | −200–−300 |

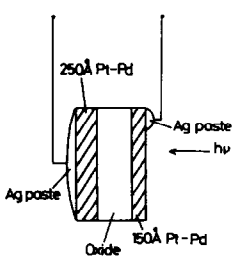


FIG. 4. Electrode system for the photoelectrical measurement.

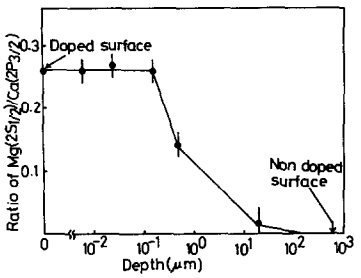


FIG. 5. Dependence of the ratio of the peak intensity of $Mg(2S_{1/2})/Ca(2P_{3/2})$ measured by XPS on the depth from the doped surface of the $CaFe_2O_4$/Na,Mg sample.

Figure 5 shows the dependence of the ratio of peak intensity of $Mg(2S_{1/2})/Ca(2P_{3/2})$ measured by XPS on the depth from the doped surface of the $CaFe_2O_4$/Na,Mg sample. The doping depth of Mg was less than about 100 $\mu$m, and the concentration of Mg decreased with depth in this region as the figure shows. Na shows the same tendency as Mg doping distribution, although a $Na(1S_{1/2})$ peak with small intensity was observed only at the doped surface because of the very small amount compared with Mg as described under Experimental. The composition of the doped surface can be roughly estimated by the analytical method using the intensity ratio reported already (*18–20*). In this analysis, the peak of $Fe(2P_{3/2})$ was also used in addition to the above peaks. The composition was roughly estimated to be $Ca_{0.8}Na_{0.2}Fe_{1.7}Mg_{0.3}O_4$. In this case, the doped surface was assumed to be the same crystal structure as Ca $Fe_2O_4$, because the same X-ray diffraction pattern as $CaFe_2O_4$ was observed for the doped surface. A small amount of Ca will be substituted for Na as well as Mg at the doped surface. In conclusion, the composition of the doped surface of the $CaFe_2O_4$/Na,Mg is similar to $Ca_{0.9}Na_{0.1}Fe_{1.8}Mg_{0.2}O_4$ except for the substitution of Ca for Mg, giving the ohmic contact.

Figure 6 shows the current–voltage curves of three samples. The voltage of the surface in the horizontal line in this figure is again referenced to the back surface. Only 2–4 $\mu$A was observed for the nondoped Ca $FeO_4$, while a large current which was independent in the direction of the bias was observed for $Ca_{0.9}Na_{0.1}Fe_{1.8}Mg_{0.2}O_4$ was shown in this figure. The small current of the nondoped $CaFe_2O_4$ is based on the large Schottky barrier at the interface of the oxide/Pt–Pd as well as the low conductivity of the bulk. On the other hand, the large current of the $Ca_{0.9}Na_{0.1}Fe_{1.8}Mg_{0.2}O_4$ is based on the ohmic contact and the high conductivity of the bulk. The one side surface doped $CaFe_2O_4$ system, i.e., Pt–Pd/Ca $Fe_2O_4$/Na,Mg/Pt–Pd system, gives the diode type I–V curve as shown in Fig. 6. Figure 7 shows the photocurrent–voltage curves of the nondoped $CaFe_2O_4$ and the $CaFe_2O_4$/Na,Mg samples. In the measurement for the latter oxide, the nondoped surface was illuminated. Only a small photocurrent ($\sim$10 $\mu A/cm^2$) was observed for $Ca_{0.9}Na_{0.1}Fe_{1.8}Mg_{0.2}O_4$ because of the nearly ohmic contact. A large photocurrent

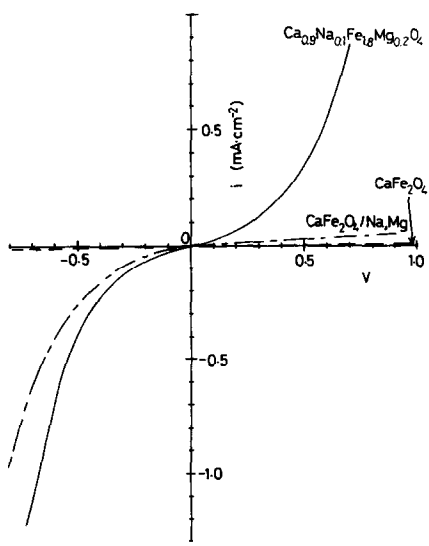


FIG. 6. I–V characteristics of $CaFe_2O_4$, $Ca_{0.9}Na_{0.1}Fe_{1.8}Mg_{0.2}O_4$, and $CaFe_2O_4$/Na,Mg in the electrode system shown in Fig. 1.

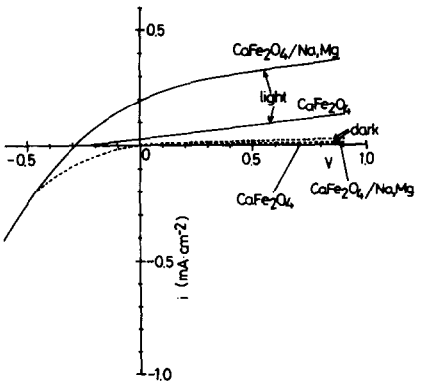


FIG. 7. Photocurrent–V characteristics of $CaFe_2O_4$ and $CaFe_2O_4$/Na,Mg in the electrode system shown in Fig. 1.

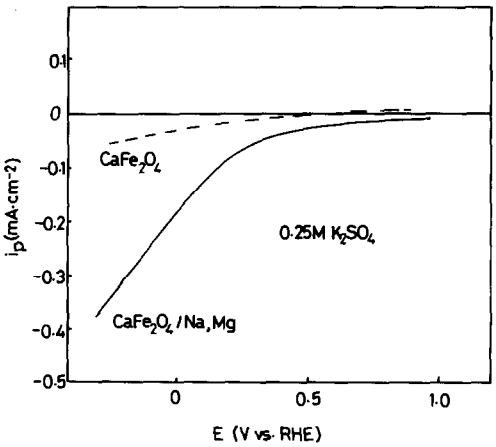


FIG. 9. Photocurrent-potential curves of the Ca $Fe_2O_4$ and the $CaFe_2O_4$/Na,Mg electrodes in 0.25 *M* $K_2SO_4$.

was observed for the $CaFe_2O_4$/Na,Mg sample, compared with the nondoped $CaFe_2O_4$ sample, as Fig. 7 shows.

Figure 8 illustrates the band models of the nondoped $CaFe_2O_4$ and the $CaFe_2O_4$/Na,Mg samples. The contact is ohmic for the $CaFe_2O_4$/Na,Mg/Pt–Pd interface, but not for the $CaFe_2O_4$/Pt–Pd interface. The diode type I–V curve and the large photocurrent observed at the $CaFe_2O_4$/Na,Mg sample, therefore, are based on the ohmic contact of $CaFe_2O_4$/Na,Mg/Pt–Pd and the relatively high conductivity of the bulk. Similar models will be applicable to the Pt–Pd/oxide/electrolyte system, as shown in Fig. 8, because similar results to Fig. 7 were observed in the electrochemical tests as shown in the latter section. In conclusion, $CaFe_2O_4$/Na,Mg is the better sample investigated here as a photocathode.

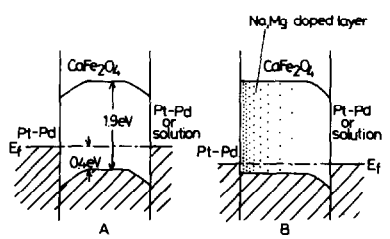


FIG. 8. Interface models of $CaFe_2O_4$ (A) and Ca $Fe_2O_4$/Na,Mg (B).

*Photoelectrochemical Properties*

Figures 9 and 10 show the photocurrent-potential curves of the nondoped $CaFe_2O_4$ and the $CaFe_2O_4$/Na,Mg electrodes in 0.25 *M* $K_2SO_4$ and 0.1 *M* $H_2SO_4$ solutions, re-

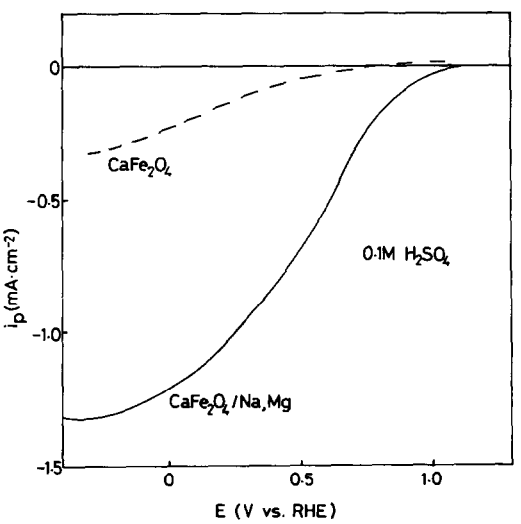


FIG. 10. Photocurrent-potential curves of the Ca $Fe_2O_4$ and $CaFe_2O_4$/Na,Mg electrodes in 0.1 *M* $H_2SO_4$.

TABLE III

AMOUNTS OF Ca AND Fe CATIONS DISSOLVED IN THE ELECTROLYTES IN 2 HR

| Charge (c) | Electrolyte | *Concentration (mole)* | | *Calculated concentration (mole)* | |
|---|---|---|---|---|---|
| | | Fe | Ca | Fe | Ca |
| 0 | 0.25 *M* $K_2SO_4$ | $<10^{-8}$ | $5\text{–}7 \times 10^{-7}$ | | |
| 0.432 | 0.25 *M* $K_2SO_4$ | $<10^{-8}$ | $5\text{–}11 \times 10^{-7}$ | | |
| 0 | 0.1 *M* $H_2SO_4$ | $5.1 \times 10^{-6}$ | $5.1 \times 10^{-6}$ | | |
| 1.612 | 0.1 *M* $H_2SO_4$ | $17.9 \times 10^{-6}$ | $11.2 \times 10^{-6}$ | $16.7 \times 10^{-6}$ | $8.35 \times 10^{-6}$ |
| | | $(12.8 \times 10^{-6})$ | $(6.1 \times 10^{-6})$ | | |

spectively. In the case of $CaFe_2O_4$/Na,Mg, the nondoped surface contacts the electrolyte. The photocurrents for the $CaFe_2O_4$/Na,Mg electrode are much larger than those for the nondoped $CaFe_2O_4$ electrode as the figures show. This is based on the ohmic contact at the $CaFe_2O_4$/Na,Mg/Pt–Pd interface and on the relatively high conductivity of the bulk, as described already. The larger photocurrent observed for acidic solution (Fig. 10) than for neutral solution (Fig. 9) is mainly attributable to the larger band bending at the former solution than at the latter solution. The change of the band bending with pH was qualitatively observed by the photovoltages as described in the previous paper (*16*). The Fermi level pinning will occur at the surface of the $CaFe_2O_4$/Na,Mg electrode, since the $1/C^2$ values obtained from the impedance measurement were independent of the potential in a Mott–Schottky plot.

The photocurrents were very stable in both solutions, since the photocurrents never decreased with the electrolyzing time. Table III shows the amounts of dissolved cations in 50-ml solutions. In the electrolysis of the electrode under illumination, the electrode potential was fixed at 0 V vs RHE. no dissolution of Fe cation was observed, but a small amount of $Ca^{2+}$ was observed in neutral solution as shown in the first column in Table III. The following chemical dissolution will occur.

$$CaFe_2O_4 + xH_2O \rightarrow Ca_{1-x}Fe_2O_{4-x} + xCa^{2+} + 2xOH^- \quad (5)$$

However, the photocathodic reaction is a $H_2$ evolution reaction in neutral solution, because no increase of the cations with the cathodic electrolysis was observed (the second column in Table III):

$$2H_2O + 2e^- \rightarrow H_2 + 2OH^-. \quad (6)$$

On the other hand, larger amounts of $Ca^{2+}$ and Fe cations were observed in acid solution as shown in Table III. The chemical dissolution was also observed for $CaFe_2O_4$ in acidic solution as shown in the third column in Table III. The ratio of Ca/Fe in the cations dissolved in the solution is about one. Therefore, the following chemical reaction will occur in acid solution.

$$5xH^+ + CaFe_2O_4 \rightarrow Ca_{1-x}Fe_{2-x}O_{4-5x/2} + xCa^{2+} + xFe^{3+} + 5x/2H_2O \quad (7)$$

The amounts of cations photoelectrochemically dissolved were obtained by subtracting the amounts of cations chemically dissolved (the third column) from the total amount of detected cations (the fourth column) and were listed in parentheses in Table III. The ratio of Ca/Fe in the cations photoelectrochemically dissolved was about 0.5. Therefore, the following reaction will occur for the photoelectrochemical dissolution of $CaFe_2O_4$:

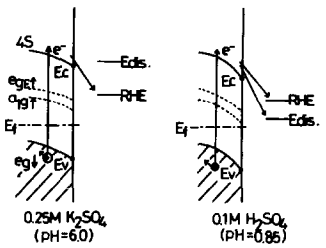


FIG. 11. Energy positions of the $CaFe_2O_4$ band and the $E_{dis}$ in acidic and neutral solutions.

$$8H^+ + CaFe_2O_4 + 2e^- \rightarrow Ca^{2+} + 2Fe^{2+} + 4H_2O. \quad (8)$$

The right side in the fourth column in Table III gives the amounts of cations calculated using Eq. (8) and the charge consumed during electrolysis shown in this table. The current efficiencies of Eq. (8) were therefore, calculated to be about 75% for the Ca $Fe_2O_4$/Na,Mg electrode. The other reaction (about 25%) is the $H_2$ evolution reaction as follows.

$$2H^+ + 2e^- \rightarrow H_2 \quad (9)$$

The photoelectrochemical dissolution of Eq. (8) occurs in preference to the $H_2$ evolution of Eq. (9) in acidic solution, while only the $H_2$ evolution reaction of Eq. (6) occurs in neutral solution as described above. The dependence of the photoelectrochemical reaction on pH at the semiconductor electrode is explained by the model proposed by Gerischer (*21*). Figure 11 illustrates the energy models of the interface of the $CaFe_2O_4$/electrolyte. If it is assumed that the flatband potential is equal to the photopotential (0.98V vs RHE in both solutions (*16*)) and that $E_f$–$E_v$ is 0.4 eV at the nondoped surface at the flatband state, the $E_c$ and $E_v$ are situated at the energy positions shown in Fig. 11, i.e., at 0.68 and 0.43 V (in pH 6.0 and pH 0.85 solutions, respectively). The energy position of the equilibrium potential of Eq. (8) ($E_{dis}$), however, cannot be calculated, because $\Delta G$ for Eq. (8) is unknown. In acid, the equilibrium potential of $H_2/H^+$ (RHE) will probably be more negative than that of the $E_{dis}$, as shown in Fig. 11. Consequently, Eq. (8) occurs in preference to the $H_2$ evolution reaction of Eq. (9). In neutral solution, the energy positions of the RHE and $E_{dis}$ will be in reverse order, because the pH dependence of the RHE and the flatband potential of the oxide are 60 mV/pH and are much smaller than that of the $E_{dis}$, which is 240 mV/pH from Eq. (8). Therefore, no photoelectrochemical dissolution occurs in neutral solution if the energy position of the $E_{dis}$ is higher than that of $E_c$ as shown in pH 6.0 solution in Fig. 11.

Thus, $CaFe_2O_4$/Na,Mg is very suitable as the *p*-type cathode material in water photolysis by a *p*/*n* assembly, if this is used in neutral solution.

## References


1. K. L. HARDEE AND A. J. BARD, *J. Electrochem. Soc.* **123,** 1024 (1976).
2. H. H. KUNG, H. S. JARRETT, A. W. SLEIGHT, AND A. FERRETTI, *J. Appl. Phys.* **48,** 2463 (1977).
3. N. A. BUTLER, D. S. GINLEY, AND M. EIBSCHUTZ, *J. Appl. Phys.* **48,** 3070 (1977).
4. D. S. GINLEY AND M. A. BUTLER, *J. Appl. Phys.* **48,** 2019 (1977).
5. M. A. BUTLER AND D. S. GINLEY, *J. Electrochem. Soc.* **125,** 228 (1978).
6. D. E. SCAIFE, *Sol. Energy* **25,** 41(1980).
7. J. H. KENNEDY, R. SHINAR, AND J. P. ZIEGLER, *J. Electrochem. Soc.* **127,** 2307 (1980).
8. J. KOENITZER, B. KHAZAI, J. HORMADALY, R. KERSHAW, K. DWIGHT, AND A. WOLD, *J. Solid State Chem.* **35,** 128 (1980).
9. N. HATANAKA, T. KOBAYASHI, H. YONEYAMA, AND H. TAMURA, *Electrochim. Acta* **27,** 1129 (1982).
10. E. POLLERT, J. HEJTMANECK, J. P. DOUMERC, J. CLAVERIE, AND P. HAGENMULLER, *J. Phys. Chem. Solids* **44,** 273 (1983).
11. K. KOCHEV, K. TZVETHOVA, AND M. GOSPODINOV, *Mater. Res. Bull.* **8,** 915 (1983).
12. A. SHAMI AND W. E. WALLACE, *Mater. Res. Bull.* **18,** 389 (1983).

*13.* J. E. TURNER, M. HENDEWERK, J. PARMETER, D. NEIMAN, AND G. A. SOMORJAI, *J. Electrochem. Soc.* **131,** 177 (1984).
*14.* Y. MATSUMOTO, M. OMAE, I. WATANABE, AND E. SOTO, *J. Electrochem. Soc.* **133,** 711 (1986).
*15.* Y. MATSUMOTO, M. OMAE, K. SUGIYAMA, AND E. SATO, *J. Phys. Chem.* **91,** 577 (1987).
*16.* Y. MATSUMOTO, K. SUGIYAMA, AND E. SATO, *J. Electrochem. Soc.*, in press.
*17.* B. F. DECKER AND J. S. KASPER, *Acta Crystallogr.* **10,** 332 (1957).
*18.* J. H. SCOFIELD, *J. Electron. Spectrosc.* **8,** 129 (1976).
*19.* D. R. PENN, *J. Electron Spectrosc.* **9,** 92 (1976).
*20.* K. HIROKAWA, M. OKU, AND F. HONDA, *Bunseki Kagaku* **26,** T8 (1977).
*21.* H. GERISCHER, *J. Electroanal. Chem.* **82,** 133 (1977).